

Millimagnitude Photometry for Transiting Extrasolar Planetary Candidates: II. Transits of OGLE-TR-113-b in the Optical and Near-IR ¹

Rodrigo F. Díaz¹, Sebastián Ramírez², José Miguel Fernández^{2,8}, José Gallardo⁷, Wolfgang Gieren³, Valentin D. Ivanov⁶, Pablo Mauas¹, Dante Minniti², Grzegorz Pietrzynski^{3,5}, Felipe Pérez², María Teresa Ruíz⁴, Andrzej Udalski⁵ and Manuela Zoccali²

ABSTRACT

We present precise V and K_s -band transit photometry for the planetary host star OGLE-TR-113. Using the K_s -band photometry, we confirm the dwarf nature of OGLE-TR-113, and obtain new estimates for its effective temperature, distance and reddening. We employ the V-band photometry to obtain planetary and orbit parameters from the transit fit, $a = (0.0232 \pm 0.0038)$ AU, orbital period $P = (1.4324752 \pm 0.0000015)$ days, $i = 86.7 - 90$, $R_p = (1.09 \pm 0.09) R_J$. These values are in excellent agreement with previous works. Assuming a mass $M_p = (1.32 \pm 0.19) M_J$ for the planet we obtain its mean density

¹Instituto de Astronomía y Física del Espacio, CONICET-Universidad de Buenos Aires, C.C. 67 Suc. 28 (1428), Buenos Aires, Argentina
E-mail: rodrigo@iafe.uba.ar, pablo@iafe.uba.ar

²Department of Astronomy, Pontificia Universidad Católica, Casilla 306, Santiago 22, Chile
E-mail: sramirez@astro.puc.cl, dante@astro.puc.cl, fperez@astro.puc.cl, mzoccali@astro.puc.cl

³Department of Physics, Universidad de Concepción, Casilla 160-C, Concepción, Chile
E-mail: pietrzyn@hubble.cfm.udec.cl, wgieren@astro-udec.cl

⁴Department of Astronomy, Universidad de Chile, Santiago, Chile
E-mail: mtruiz@das.uchile.cl

⁵Warsaw University Observatory, Al. Ujazdowskie 4, 00-478 Warszawa, Poland
E-mail: udalski@astrouw.edu.pl

⁶European Southern Observatory, Vitacura, Santiago, Chile
E-mail: vivanov@eso.org

⁷CNRS UMR 5574, CRAL, École normale supérieure, 69364, Lyon Cedex 07, France
E-mail: jose.gallardo@ens-lyon.fr

⁸Harvard CFA, USA
E-mail: jfernand@cfa.harvard.edu

$\rho = (1.26 \pm 0.50) \text{ g cm}^{-3}$, also in agreement with previous works. The transit observed in the K_s -band has a larger scatter and we find its amplitude to be consistent with that in the V-band. In this way, we find an independent confirmation of the planetary nature of OGLE-TR-113b.

Subject headings: planets and satellites: individual (OGLE-TR-113b) – stars: individual (OGLE-TR-113)

1. Introduction

The discovery of hot Jupiters that transit in front of their parent stars has advanced our knowledge of extrasolar planets adding a fundamental datum: the planetary radius. Besides, combined with radial velocity measurements, it allows a precise measurement of the companion mass, and therefore, its mean density. This observational data are fundamental for the development of models. New samples of transiting hot Jupiters should become available soon (see, for example, Bordé et al. 2003 (COROT); Alonso et al. 2004 and O’Donovan et al. 2006a (TrES); Bakos et al. 2004 (HAT); Fischer et al. 2005 (N2K); Pollacco et al. 2006 (WASP); McCullough et al. 2005 (XO); Aigrain et al. 2006 and Irwin et al. 2006 (Monitor); Holman et al. 2006 (TLC); Sahu et al. 2006 (SWEEPS)) but up to now the Optical Gravitational Lensing Experiment (OGLE) has provided the largest number of transiting candidates (Udalski et al. 2002a,b,c, 2003). In particular, Udalski et al. (2002b) discovered transits in the $I = 14.42$ magnitude star OGLE-TR-113, located in the Carina region of the Milky Way disk, at $\text{RA}(2000) = 10^{\text{h}}52^{\text{m}}24''.40$, $\text{DEC}(2000) = -61^{\circ}26'48''.5$. They monitored 10 individual transits, measuring an amplitude $\Delta I = 0.030$ mag, and a period $P = 1.43250$ days.

The planetary nature of the transiting candidate OGLE-TR-113b was confirmed by Bouchy et al. (2004) and Konacki et al. (2004) using high precision radial velocities measurements. The results are shown in Table 1 and confirm that OGLE-TR-113b can be classified as a Very Hot Jupiter. Recently, Gillon et al. (2006) and Snellen & Covino (2006) presented R and K-band transit photometry, respectively. They obtain parameters in excellent agreement with previous works. Additionally, Snellen & Covino (2006) report a tentative detection of emission from the planet.

¹Based on observations collected with the Very Large Telescope at Paranal Observatory (JMF and DM visiting observers), and at the ESO New Technology Telescope at La Silla Observatory (SR, FP and DM visiting observers) for the ESO Programmes 075.C-0427, 075.B-0414, and 076.C-0122.

There are many difficulties to confirm real planets among the low amplitude transit objects discovered by photometric transit searches. Most of the candidates turn out to be grazing binaries, low mass stars, triples or blends (see, for example, Torres et al. 2005; Pont et al. 2005; Mandushev et al. 2005; O’Donovan et al. 2006b). Furthermore, the red noise sometimes causes false detections (Pont et al. 2006b). Therefore, real planets must be confirmed with accurate radial velocities, which in the case of the OGLE candidates is difficult because their magnitudes range from $V=15$ to 18 and they are located in very crowded fields.

Another test to check the real planetary nature of low amplitude transiting objects is to observe their transits in different wavelengths. To first order, ignoring stellar limb darkening, the transit amplitudes should be achromatic, i.e. they should be similar in the V, I, and K_s -bands. Large amplitude differences would be indicative of blends.

A triple system where a low mass star transits in front of a solar type star that is blended with a foreground red star would give larger amplitudes in the K_s -band. On the other hand, if the blend is with an early type star in the foreground, the amplitudes would be larger in the V-band. Unfortunately, blends with foreground stars of similar color as the eclipsed star would yield similar transit depths in all bands. In this sense, while multicolor transit photometry can help to discriminate most impostors, it cannot be regarded as final proof of the true nature of the planetary companion (see Moutou et al. 2005).

To second order, the multiple wavelength observations allow to test limb darkening coefficients. This is so because the shapes of the transit light curves vary with wavelength due to stellar limb darkening and to a possible planetary atmosphere (Burrows et al. 2000).

We have undertaken an observational project at the ESO telescopes at La Silla and Paranal Observatories, to measure transit depths in the K_s and V-bands, to compare with the OGLE I-band observations. In the first paper we presented optical photometry of the planetary transit candidate OGLE-TR-109b (Fernández et al. 2006, hereafter Paper I) . Other papers in the series discuss OGLE-TR-111 (Minniti et al. 2007) and OGLE-TR-82 (Hoyer et al. 2007).

In this work we present new photometry covering a transit of OGLE-TR-113b in the V-band with the ESO VLT, and another transit in the K_s -band with the ESO NTT, improving the measurements of the planetary parameters. The present observations allow to check independently and to refine the ephemeris and amplitudes, and to determine variations on the radius measurement using different photometric filters.

There is a fundamental difference in our observations with respect to OGLE. The OGLE candidates have light curves made of several transits. While there are relatively few OGLE

I-band points per transit, the final phased light curves are very clean, and representative of an average transit. Our data show single transits but very well sampled. As such, they could in principle be sensitive to large planetary satellites, for example (Charbonneau et al. 2000a).

This paper is organized as follows. Sections 2 and 3 present the infrared and optical observations and photometry, respectively. Section 4 discusses the parameters of the target derived from the present observations. Finally, the conclusions are outlined in Section 5.

2. IR Observations and Photometry

2.1. IR Observations and Data Reduction

OGLE-TR-113 was observed during the nights of May 4 and 5, 2005, using the SOFI IR camera and spectrograph at the ESO NTT. SOFI is equipped with a Hawaii HgCdTe detector of 1024×1024 pixels, characterized by a 5.4 e/ADU gain, a readout noise of 2.1 ADU and a dark current of less than 0.1 e/sec. We used it in the Large Field camera mode, giving a 4.9×4.9 arcmin² field. All measurements were made through the K_s -band filter ($\lambda_0 = 2.162 \mu\text{m}$ and $\Delta\lambda = 0.275 \mu\text{m}$). In Figure 1 we show a 12×12 arcsec² portion of an image acquired with SOFI.

We monitored several OGLE candidates (OGLE-TR-108, OGLE-TR-109, OGLE-TR-113, OGLE-TR-170, and OGLE-TR-171), being in some cases limited by the weather (high wind and clouds). The telescope was slightly defocussed to avoid saturation of the detector for the brightest stars. This does not affect the differential aperture photometry nor our final results.

The reductions were made using IRAF tasks ². First of all, the crosstalk correction was applied, taking into account the detectors sensitivity difference between the upper and lower half. Then the sky subtraction was applied. The whole dataset was acquired using "dither-5" around two offset positions that included the target. These contiguous sky images were used to generate local skies close in time for each of the offset images. Then the appropriately scaled skies were subtracted from the images. Finally, we applied flat-field corrections to all images and aligned them. For the flat-fields, we used the correction images provided by

²IRAF is distributed by the National Optical Observatories, operated by Universities for Research in Astronomy, Inc.

the NTT SciOps team³, and the alignment was done with *lintran* and *imshift*.

The calibration of the IR photometry was made using 2MASS. There were a dozen stars in common located in the OGLE-TR-113 field (not including this star because it is not listed as a 2MASS source). Discarding outliers, we selected the 10 most isolated stars with $12 < K_s < 14.5$, obtaining $\text{RMS}_K = 0.03$. The zero point of the K_s -band photometry should be good to 0.1 mag, which is accurate enough for our purposes. We also checked this calibration against the DENIS sources in the field, finding excellent agreement. Finally, we find $K_s = 13.0 \pm 0.1$ and $V - K_s = 3.5 \pm 0.1$ for this star. The resulting light curve is shown in Figure 2.

2.2. IR photometry

Stellar parameters

Based on the high dispersion spectroscopy, Konacki et al. (2004) classify OGLE-TR-113 as a K-type main sequence star with $T_{\text{eff}} = 4800 \pm 150$ K, gravity $\log g = 4.5$, and metallicity $[\text{Fe}/\text{H}] = +0.0$ dex. They estimate the star is located at a distance of about 600 pc. They adopt for this star a mass of $M_* = 0.79 \pm 0.06 M_\odot$, and a radius $R_* = 0.78 \pm 0.06 R_\odot$, very similar to the more recent values presented by Gillon et al. (2006), who used spectroscopic measurements to obtain the primary mass ($M_* = 0.78 \pm 0.02 M_\odot$), and R-band high precision transit photometry to obtain the stellar radius ($R_* = 0.77 \pm 0.02 R_\odot$). Recently, Santos et al. (2006) derived similar stellar parameters for OGLE-TR-113: temperature $T_{\text{eff}} = 4804 \pm 106$ K, gravity $\log g = 4.52 \pm 0.26$, metallicity $[\text{Fe}/\text{H}] = +0.15 \pm 0.10$ dex, based on high dispersion spectroscopy. They also derived the distance $d = 553$ pc, and an absorption $A_V = 0.42$ based on the OGLE photometry. The values from these two independent studies agree within the uncertainties.

With the present optical and IR photometry we can confirm independently some of these parameters: the spectral type, luminosity, mass, radius and distance.

In a previous work, we have used optical and infrared photometry to characterize OGLE extrasolar planetary companions using surface brightness analysis (Gallardo et al. 2005). Unfortunately, at the time we did not have K_s -band photometry of OGLE-TR-113. Following the analysis described in that work, we obtained from the IR photometry surface brightness the following stellar parameters: temperature $T_{\text{eff}} = 4396 \pm 50$ K, radius $R_* = 0.81 \pm 0.05$

³www.ls.eso.org/lasilla/sciops/ntt/sofi/reduction/flat_fielding.html

R_{\odot} , distance $d = 550 \pm 30$ pc, and reddening $E_{(B-V)} = 0.17 \pm 0.01$ mag (see Figure 3). In spite of the lower temperature, the distance and reddening are similar to those measured by Santos et al. (2006), and the radius is similar to that of Gillon et al. (2006). The determined distance of 550 pc is consistent with the K_s -band photometry, making this the nearest known OGLE planet. This is also the smallest OGLE star with a confirmed planet.

Figure 4 shows the optical and IR CMDs for the stars in a $1' \times 1'$ field centered on OGLE-TR-113. The filled red square represents the extrasolar host star OGLE-TR-113. Additionally, we show isochrones for solar age and metallicity for three different distances, calculated using the value for colour excess and extinction determined above (J. Gallardo, private communication). The disk main sequence is very well defined, and the position of the target star is consistent with a dwarf star, despite being apparently located away from the main sequence, indicating that either this is a nearby K-dwarf, or a subgiant located farther than the majority of the stars in this field. We prefer the first option based on the independent evidence from the spectroscopy. For example, a K0V star has $M_{K_s} = 3.9$, and a K5V star has $M_{K_s} = 4.7$ (Cox 2000). These give $K_s = 12.8$ and 13.6 for a distance of 600 pc, neglecting interstellar dust extinction.

3. Optical Observations and Photometry

3.1. Optical Observations and data reduction

The observations and photometry are described in detail in Paper I. Photometric observations were taken with VIMOS at the Unit Telescope 4 (UT4) of the European Southern Observatory Very Large Telescope (ESO VLT) at Paranal Observatory during the nights of April 9 to 12, 2005. The VIMOS field of view consists of four CCDs, each covering 7×8 arcmin, with a separation gap of 2 arcmin, and a pixel scale of 0.205 arcsec/pixel. Since the scope of the observations is to detect new transit candidates, we monitored four different fields. A number of OGLE transit candidates located in the observed fields were monitored simultaneously. OGLE-TR-113 happened to have a transit towards the end of the second night of our run.

Clearly, there exists a compromise between the temporal resolution of the observations and the number of fields monitored. The observations presented here were carried out alternating between two different fields, observing three 15 sec exposures on each one. For this program we managed to reduce the observation overheads for telescope presets, instrument setups, and the telescope active optics configuration to an absolute minimum. This ensured adequate sampling of the transit providing at the same time > 10000 stars with

$15 < V < 19$ for which lightcurves can be obtained. If individual candidates are to be observed a much better temporal resolution can be achieved using other telescopes or instruments (see Gillon et al. (2006) for an example of high-temporal resolution observations with NTT/SUSI and Pont et al. (2006a) for observations of OGLE-TR-10 and OGLE-TR-56 acquired with VLT/FORS.) We obtained 150 points in the field of OGLE-TR-113 during the second night. The observations lasted for about 9.5 hours, until the field went below 3 airmasses.

We used the Bessell V filter of VIMOS, with $\lambda_0 = 5460 \text{ \AA}$, $\text{FWHM} = 890 \text{ \AA}$. The V-band was chosen in order to complement the OGLE light curves which are made with the I-band filter. In addition, the V-band is more sensitive to the effects of limb darkening during the transit, and is adequate for the modeling of the transit parameters.

Figure 5 shows a $12 \times 12 \text{ arcsec}^2$ portion of a 0.6 arcsec seeing image, illustrating that the candidate star is unblended. There are a $V = 16.0 \text{ mag}$ star 2 arcsec East and a $V = 17.5 \text{ mag}$ star 2 arcsec West of our target. These do not affect our photometry.

3.2. V-band transit photometry

In order to reduce the analysis time of the vast dataset acquired with VIMOS, the images of OGLE-TR-113 analyzed here are $400 \times 400 \text{ pix}$, or 80 arcsec on a side. Each of these small images contains about 500 stars with $15 < V < 24$ that can be used by the software ISIS for the differential photometry, and in the light curve analysis. The best seeing images ($\text{FWHM} = 0.6 \text{ arcsec}$) taken near the zenith were selected, and a master image was made in order to serve as reference for the difference image analysis (see Alard & Lupton 1998; Alard 2000).

The seeing, position of the stars, peak counts, and sky counts were monitored. The individual light curves were checked against these parameters in search for systematic effects. Extensive tests with the difference image photometry were performed, varying different photometric parameters and choosing different sets of reference stars. The software gives relative fluxes that are dependent on the reference stars used, so that the final amplitude was measured using aperture photometry in the individual images. To do this we selected three images centered on the transit and three images before the transit acquired with similar seeing but different airmass. Following this procedure we believe that the measurement of the transit amplitude is reliable.

The photometry of OGLE-TR-113, with mean $V = 16.08$ gives $\text{RMS}_V = 0.0015$ to 0.0024 mag throughout the second night of the run. This quantity is found to correlate

mostly with the sizes of the point sources, given by a combination of seeing and airmass. Therefore, the photometric scatter increased for the end of the night, when the transit occurred (see Figure 6).

Figure 7 shows the full light curve for the second night of observations, when the OGLE-TR-113 transit was monitored. For comparison we also show the phased light curve of the OGLE I-band photometry (in a similar scale) in the same Figure. The transit is well sampled in the V-band, and the scatter is smaller. There are $N_t = 30$ points in our single transit, shown in Figure 8. The minimum is well sampled, allowing us to measure an accurate amplitude. In the case of OGLE, the significance of the transits is –in part– judged by the number of transits detected. In the case of the present study, we compute the signal-to-noise of the single, well sampled transit. For a given photometric precision of a single measurement of σ_p and a transit depth ΔV , this signal-to-noise transit is $S/N = N_t^{1/2} \Delta V / \sigma_p$ (Gaudi 2005). For OGLE-TR-113 we find the S/N of this transit to be $S/N \approx 76$ using $\Delta V = 0.025$ and $\sigma_p = 0.0018$.

The resulting light curve was corrected for a linear trend and phased adopting a period of $P = 1.4324758$ days from Konacki et al. (2004). The curve was fitted using transit curves computed with the algorithms of Mandel & Agol (2002). The curves depend on the ratio between the planetary and the stellar radii, the ratio between orbit radius and stellar radius, the inclination angle and the coefficients of the limb darkening model chosen. All parameters were fitted simultaneously, with a quadratic model for the limb darkening. We found that within the errors the limb darkening coefficients remain the same as those presented by Claret (2000) ($u_1 = 0.73$, $u_2 = 0.092$) for the stellar parameters, which were also employed by Gillon et al. (2006): $T_{\text{eff}} = 4750\text{K}$, metallicity $[M/H] = 0.0$, surface gravity $\log g = 4.5$ and microturbulence velocity $\xi_t = 1.0 \text{ km/s}$. Therefore, the coefficients were fixed at those values in order to minimize computation time. The best fit to the transit is shown in Figure 8 as a solid line.

The uncertainties of the fit parameters were estimated from the χ^2 hypersurface. In the case of non-linear model fitting like this it is customary to obtain the parameters errors from the intersection of the χ^2 hypersurface with a constant hyperplane defined by $\chi^2 = \chi_{bf}^2 + 1$, where χ_{bf}^2 is the value of χ^2 associated with the best fit. However, as shown by Pont et al. (2006b), the existence of correlation between the observations produces a low-frequency noise which must be considered to obtain a realistic estimation of the uncertainties. To model the covariance we followed Gillon et al. (2006) and obtained an estimate of the systematic errors in our observations from the residuals of the light curve. The amplitude of the white (σ_w) and red (σ_r) noise can be obtained by solving the following system of equations:

$$\sigma_1^2 = \sigma_w^2 + \sigma_r^2 \quad (1)$$

$$\sigma_8^2 = \frac{\sigma_w^2}{8} + \sigma_r^2, \quad (2)$$

where σ_1 is the standard deviation taken over single residual points and σ_8 is the standard deviation taken over a sliding average over eight points. We estimated the white noise amplitude, $\sigma_w = 2.1$ mmag, and the low-frequency red noise amplitude, $\sigma_r = 0.2$ mmag.

Then, we assume that the $1\text{-}\sigma$ uncertainty intervals are determined by the surface defined by the equation (see Gillon et al. 2006, Eq. 7):

$$\chi^2 = \chi_{bf} + \Delta\chi^2 = \chi_{bf} + 1 + N_t \frac{\sigma_r^2}{\sigma_w^2}, \quad (3)$$

where N_t is the number of points in the transit. Using the value for σ_r , σ_w , and N_t mentioned above, we obtained $\Delta\chi^2 = 1.25$. The projections of this surface are shown in Figure 9. The parameters and uncertainty intervals obtained with this method are:

$$\begin{aligned} a/R_* &= 6.48 \pm 0.90 \\ R_p/R_* &= 0.1455 \pm 0.0083 \\ i &= 86.66 \pm 3.34, \end{aligned} \quad (4)$$

where a is the orbit radius, R_p and R_* are the planetary and stellar radius, respectively and i is the orbital inclination angle.

We also fitted the lightcurve to obtain a refined ephemeris for the transit times. The parameters obtained above were held fixed and the time at mean transit was fitted alone. Using the ephemeris presented by Konacki et al. (2004) we also measure a refined period. Our refined ephemeris for the mean transit times of OGLE-TR113b is:

$$HJD(\text{middle of transit}) = 2453471.77836(34) + 1.4324752(15) \times E,$$

where the numbers given in parentheses are the uncertainties in the last digits, about 30 seconds for the central time and 0.2 seconds for the period. The obtained ephemeris agrees with those from previous works (Konacki et al. 2004; Gillon et al. 2006; Snellen & Covino 2006).

4. The Radius and other parameters of OGLE-TR-113-b

There are 20 giant planets with well measured radii to date (November 2006). These are the Solar system planets Jupiter, Saturn, Uranus and Neptune, plus the extrasolar planets OGLE-TR-10 (Konacki et al. 2005), OGLE-TR-56 (Konacki et al. 2003), OGLE-TR-111 (Pont et al. 2004), OGLE-TR-113 (Bouchy et al. 2004; Konacki et al. 2004; Gillon et al.

2006, and this work), OGLE-TR-132 (Bouchy et al. 2004), HD209458 (Charbonneau et al. 2000b; Henry et al. 2000), HD189733 (Bouchy et al. 2005), HD149026 (Sato et al. 2005), TrES-1 (Alonso et al. 2004), TrES-2 (O’Donovan et al. 2006a), X0-1 (McCullough et al. 2006), HAT-P-1 (Bakos et al. 2006), WASP-1 and WASP-2 (Collier Cameron et al. 2006). Finally, two more hot Jupiter planets out of 16 bonafide transiting candidates named SWEEPS-4 and SWEEPS-11 have been discovered by Sahu et al. (2006) in the Galactic bulge.

Our temporal resolution is not enough to obtain an accurate solution for all the parameters of the system. In particular, the sampling of the ingress and egress is not high enough to allow the breaking of the degeneracy between stellar radius and orbital inclination. Indeed, assuming a stellar mass of $M_* = (0.78 \pm 0.02) M_\odot$, the error on the primary radius obtained from our lightcurve using Kepler’s third law is around 15% ($R_* = (0.76 \pm 0.12) R_\odot$). Therefore, to obtain the planetary parameters from the V-band fit parameters (see Equations 4) we relied on the accurate value for stellar radius given by Gillon et al. (2006): $R_* = (0.77 \pm 0.02) R_\odot$. The obtained parameters are shown in Table 1, together with those obtained in previous works. Note that due to our poorer temporal resolution the uncertainty intervals are larger than those presented in previous studies. Nevertheless, there exists an excellent agreement with all previous works.

In order to measure the radius accurately, we rely on the optical photometry. Obviously, the K_s -band photometry shows larger scatter, and even though we see the whole transit, there is not enough baseline covered. Using the IR transit, it is possible to derive parameters for the planetary companion to check for consistency only. We fit two lines, one for the out-transit data and another for the in-transit one, keeping zero the slope of the curve. The difference between the intercepts of each straight line equals the depth of the transit. For OGLE-TR-113 we obtained $\Delta K_S = 0.035 \pm 0.009$, from which we derive $R_p = 1.4 \pm 0.2 R_J$. Clearly the error is large, but we find a value consistent with the more accurate V-band observations. The transits in the I, V and K_s band are shown together for comparison in Figure 10.

5. Conclusions

We studied the OGLE-TR-113 star-planet system using optical and IR photometry. We have produced an independent confirmation of the dwarf nature of OGLE-TR-113 by studying the IR and optical CMDs in the observed fields.

We observed two transits of planet OGLE-TR-113-b. The first was observed in the V-band with VIMOS at the ESO VLT and the second in the K_s -band with SOFI at the ESO

NTT. There are 30 and 40 points per transit respectively. The quality of the photometry obtained with VIMOS is superb, with dispersion comparable to photon noise. Therefore, processing the complete VIMOS dataset should provide an interesting opportunity to identify new transit candidates around 2 magnitudes fainter than those from the OGLE survey.

We compared our observations with those from previous works (Udalski et al. 2003; Gillon et al. 2006), and confirmed that the transit amplitudes in the V, I, and R-bands are similar, consistent with the planetary nature of the transiting companion. The K_s -band photometry also shows clearly the transit, although with a large scatter and insufficient baseline. Within the larger errors, the parameters are consistent with the more accurate V-band observations.

We checked the limb darkening coefficients using the V-band photometry and found the values presented by Claret (2000) were adequate. However, we were not able to put strong constraints to the coefficients in the K_s -band, since our light curve is not accurate enough.

Finally, the planetary parameters obtained from the V-band photometry with assumed stellar radius $R_* = 0.77 R_\odot$ are in excellent agreement with those presented in the cited works (Konacki et al. 2004; Bouchy et al. 2004; Gillon et al. 2006). We measured the orbit radius $a = (0.0232 \pm 0.0038)$ AU, the orbital period $P = (1.4324752 \pm 0.0000015)$ days, the inclination angle $i = (86.66 \pm 3.34)$ degrees and the planetary radius $R_p = (1.09 \pm 0.09) R_J$, which for $M_p = (1.32 \pm 0.19) M_J$, gives the planet mean density $\rho = (1.26 \pm 0.50) \text{ g cm}^{-3}$.

DM, JMF, GP, MZ, MTR, WG are supported by Fondap Center for Astrophysics No. 15010003. DM was also supported by a Fellowship from the John Simon Guggenheim Foundation. AU acknowledges support from the Polish MNSW DST grant to the Warsaw University Observatory. We thank the ESO staff at Paranal Observatory.

REFERENCES

- Aigrain, S., Hodgkin, S., Irwin, J., Hebb, L., Irwin, M., Favata, F., Moraux, E., & Pont, F. 2006, MNRAS, in press (astro-ph/0611431)
- Alard, C. 2000, A&AS, 144, 363
- Alard, C., & Lupton, R. H. 1998, ApJ, 503, 325
- Alonso, R., Brown, T. M., Torres, G., Latham, D. W., Sozzetti, A., Mandushev, G., Belmonte, J. A., Charbonneau, D., Deeg, H. J., Dunham, E. W., O’Donovan, F. T., & Stefanik, R. P. 2004, ApJ, 613, L153

- Bakos, G., Noyes, R. W., Kovács, G., Stanek, K. Z., Sasselov, D. D., & Domsa, I. 2004, *PASP*, 116, 266
- Bakos, G. A., Noyes, R. W., Kovacs, G., Latham, D. W., Sasselov, D. D., Torres, G., Fischer, D. A., Stefanik, R. P., Sato, B., Johnson, J. A., Pal, A., Marcy, G. W., Butler, R. P., Esquerdo, G. A., Stanek, K. Z., Lazar, J., Papp, I., Sari, P., & Sipocz, B. 2006, *ApJ*, accepted (astro-ph/0609369)
- Bordé, P., Rouan, D., & Léger, A. 2003, *A&A*, 405, 1137
- Bouchy, F., Pont, F., Santos, N. C., Melo, C., Mayor, M., Queloz, D., & Udry, S. 2004, *A&A*, 421, L13
- Bouchy, F., Udry, S., Mayor, M., Moutou, C., Pont, F., Iribarne, N., da Silva, R., Ilovaisky, S., Queloz, D., Santos, N. C., Ségransan, D., & Zucker, S. 2005, *A&A*, 444, L15
- Burrows, A., Guillot, T., Hubbard, W. B., Marley, M. S., Saumon, D., Lunine, J. I., & Sudarsky, D. 2000, *ApJ*, 534, L97
- Charbonneau, D., Brown, T. M., Latham, D. W., & Mayor, M. 2000a, *ApJ*, 529, L45
- . 2000b, *ApJ*, 529, L45
- Claret, A. 2000, *A&A*, 363, 1081
- Collier Cameron, A., Bouchy, F., Hebrard, G., Maxted, P., Pollacco, D., Pont, F., Skillen, I., Smalley, B., Street, R. A., West, R. G., Wilson, D. M., Aigrain, S., Christian, D. J., Clarkson, W. I., Enoch, B., Evans, A., Fitzsimmons, A., Gillon, M., Haswell, C. A., Hebb, L., Hellier, C., Hodgkin, S. T., Horne, K., Irwin, J., Kane, S. R., Keenan, F. P., Loeillet, B., Lister, T. A., Mayor, M., Moutou, C., Norton, A. J., Osborne, J., Parley, N., Queloz, D., Ryans, R., Triaud, A. H. M. J., Udry, S., & Wheatley, P. J. 2006, *MNRAS*, accepted (astro-ph/0609688)
- Cox, A. N. 2000, *Allen’s astrophysical quantities* (Allen’s astrophysical quantities, 4th ed. Publisher: New York: AIP Press; Springer, 2000. Edited by Arthur N. Cox. ISBN: 0387987460)
- Fernández, J. M., Minniti, D., Pietrzynski, G., Gieren, W., Ruíz, M. T., Zoccali, M., Udalski, A., & Szeifert, T. 2006, *ApJ*, 647, 587, (Paper I)
- Fischer, D. A., Laughlin, G., Butler, P., Marcy, G., Johnson, J., Henry, G., Valenti, J., Vogt, S., Ammons, M., Robinson, S., Spear, G., Strader, J., Driscoll, P., Fuller, A., Johnson, T., Manrao, E., McCarthy, C., Muñoz, M., Tah, K. L., Wright, J., Ida, S., Sato, B., Toyota, E., & Minniti, D. 2005, *ApJ*, 620, 481

- Gallardo, J., Minniti, D., Valls-Gabaud, D., & Rejkuba, M. 2005, *A&A*, 431, 707
- Gaudi, B. S. 2005, *ApJ*, 628, L73
- Gillon, M., Pont, F., Moutou, C., Bouchy, F., Courbin, F., Sohy, S., & Magain, P. 2006, *A&A*, 459, 249
- Henry, G. W., Marcy, G. W., Butler, R. P., & Vogt, S. S. 2000, *ApJ*, 529, L41
- Holman, M. J., Winn, J. N., Latham, D. W., O’Donovan, F. T., Charbonneau, D., Bakos, G. A., Esquerdo, G. A., Hergenrother, C., Everett, M. E., & Pál, A. 2006, *ApJ*, 652, 1715
- Hoyer, S., Ramírez, S., Minniti, D., Pietrzynski, G., Ruíz, M. T., Gieren, W., Ivanov, V. D., Udalski, A., Zoccali, M., Díaz, R. F., Pérez, F., Fernández, J. M., Gallardo, J., Rejkuba, M., & Carrasco, R. 2007, in preparation
- Irwin, J., Irwin, M., Aigrain, S., Hodgkin, S., Hebb, L., & Moraux, E. 2006, *MNRAS*, accepted (astro-ph/0612395)
- Konacki, M., Torres, G., Jha, S., & Sasselov, D. D. 2003, *Nature*, 421, 507
- Konacki, M., Torres, G., Sasselov, D. D., & Jha, S. 2005, *ApJ*, 624, 372
- Konacki, M., Torres, G., Sasselov, D. D., Pietrzyński, G., Udalski, A., Jha, S., Ruiz, M. T., Gieren, W., & Minniti, D. 2004, *ApJ*, 609, L37
- Mandel, K., & Agol, E. 2002, *ApJ*, 580, L171
- Mandushev, G., Torres, G., Latham, D. W., Charbonneau, D., Alonso, R., White, R. J., Stefanik, R. P., Dunham, E. W., Brown, T. M., & O’Donovan, F. T. 2005, *ApJ*, 621, 1061
- McCullough, P. R., Stys, J. E., Valenti, J. A., Fleming, S. W., Janes, K. A., & Heasley, J. N. 2005, *PASP*, 117, 783
- McCullough, P. R., Stys, J. E., Valenti, J. A., Johns-Krull, C. M., Janes, K. A., Heasley, J. N., Bye, B. A., Dodd, C., Fleming, S. W., Pinnick, A., Bissinger, R., Gary, B. L., Howell, P. J., & Vanmunster, T. 2006, *ApJ*, 648, 1228
- Minniti, D., Fernández, J. M., Díaz, R. F., Udalski, A., Pietrzynski, G., Gieren, W., Rojo, P., Ruíz, M. T., Zoccali, M., & Szeifert, T. 2007, *ApJ*, submitted

- Moutou, C., Pont, F., Barge, P., Aigrain, S., Auvergne, M., Blouin, D., Cautain, R., Erikson, A. R., Guis, V., Guterman, P., Irwin, M., Lanza, A. F., Queloz, D., Rauer, H., Voss, H., & Zucker, S. 2005, *A&A*, 437, 355
- O’Donovan, F. T., Charbonneau, D., Mandushev, G., Dunham, E. W., Latham, D. W., Torres, G., Sozzetti, A., Brown, T. M., Trauger, J. T., Belmonte, J. A., Rabus, M., Almenara, J. M., Alonso, R., Deeg, H. J., Esquerdo, G. A., Falco, E. E., Hillenbrand, L. A., Roussanova, A., Stefanik, R. P., & Winn, J. N. 2006a, *ApJ*, 651, L61
- O’Donovan, F. T., Charbonneau, D., Torres, G., Mandushev, G., Dunham, E. W., Latham, D. W., Alonso, R., Brown, T. M., Esquerdo, G. A., Everett, M. E., & Creevey, O. L. 2006b, *ApJ*, 644, 1237
- Pollacco, D. L., Skillen, I., Cameron, A. C., Christian, D. J., Hellier, C., Irwin, J., Lister, T. A., Street, R. A., West, R. G., Anderson, D., Clarkson, W. I., Deeg, H., Enoch, B., Evans, A., Fitzsimmons, A., Haswell, C. A., Hodgkin, S., Horne, K., Kane, S. R., Keenan, F. P., Maxted, P. F. L., Norton, A. J., Osborne, J., Parley, N. R., Ryans, R. S. I., Smalley, B., Wheatley, P. J., & Wilson, D. M. 2006, *PASP*, 118, 1407
- Pont, F., Bouchy, F., Queloz, D., Santos, N. C., Melo, C., Mayor, M., & Udry, S. 2004, *A&A*, 426, L15
- Pont, F., Melo, C. H. F., Bouchy, F., Udry, S., Queloz, D., Mayor, M., & Santos, N. C. 2005, *A&A*, 433, L21
- Pont, F., Moutou, C., Gillon, M., Udalski, A., Bouchy, F., Fernandes, J., Gieren, W., Mayor, M., Mazeh, T., Minniti, D., Melo, C., Naef, D., Pietrzynski, G., Queloz, D., Ruiz, M. T., Santos, N., & Udry, S. 2006a, *A&A*, submitted (astro-ph/0610827)
- Pont, F., Zucker, S., & Queloz, D. 2006b, *MNRAS*, 373, 231
- Sahu, K. C., Casertano, S., Bond, H. E., Valenti, J., Ed Smith, T., Minniti, D., Zoccali, M., Livio, M., Panagia, N., Piskunov, N., Brown, T. M., Brown, T., Renzini, A., Rich, R. M., Clarkson, W., & Lubow, S. 2006, *Nature*, 443, 534
- Santos, N. C., Pont, F., Melo, C., Israelian, G., Bouchy, F., Mayor, M., Moutou, C., Queloz, D., Udry, S., & Guillot, T. 2006, *A&A*, 450, 825
- Sato, B., Fischer, D. A., Henry, G. W., Laughlin, G., Butler, R. P., Marcy, G. W., Vogt, S. S., Bodenheimer, P., Ida, S., Toyota, E., Wolf, A., Valenti, J. A., Boyd, L. J., Johnson, J. A., Wright, J. T., Ammons, M., Robinson, S., Strader, J., McCarthy, C., Tah, K. L., & Minniti, D. 2005, *ApJ*, 633, 465

- Snellen, I. A. G., & Covino, E. 2006, MNRAS, accepted (astro-ph/0611877)
- Torres, G., Konacki, M., Sasselov, D. D., & Jha, S. 2005, ApJ, 619, 558
- Udalski, A., Paczynski, B., Zebrun, K., Szymanski, M., Kubiak, M., Soszynski, I., Szewczyk, O., Wyrzykowski, L., & Pietrzynski, G. 2002a, Acta Astronomica, 52, 1
- Udalski, A., Pietrzynski, G., Szymanski, M., Kubiak, M., Zebrun, K., Soszynski, I., Szewczyk, O., & Wyrzykowski, L. 2003, Acta Astronomica, 53, 133
- Udalski, A., Szewczyk, O., Zebrun, K., Pietrzynski, G., Szymanski, M., Kubiak, M., Soszynski, I., & Wyrzykowski, L. 2002b, Acta Astronomica, 52, 317
- Udalski, A., Zebrun, K., Szymanski, M., Kubiak, M., Soszynski, I., Szewczyk, O., Wyrzykowski, L., & Pietrzynski, G. 2002c, Acta Astronomica, 52, 115

Table 1: Planetary Parameters

	This work	Guillon et al.(2006)	Bouchy et al.(2004)	Konacki et al.(2004)
Inclination Angle (deg)	86.7 – 90	88.8 – 90	85 – 90	88.4 ± 2.2
Period (days)	1.4324752 ± 0.0000015	1.4324757 ± 0.0000013	1.43250 (adopted)	1.4324758 ± 0.0000046
Orbit Radius (AU)	0.0232 ± 0.0038	0.0229 ± 0.0002	0.0228 ± 0.0006	0.02299 ± 0.00058
Planet mass (M _J)	1.32 ± 0.19 (adopted)	1.32 ± 0.19	1.35 ± 0.22	1.08 ± 0.28
Planet radius (R _J)	1.09 ± 0.09	1.09 ± 0.03	1.08 ^{+0.07} _{-0.05}	1.09 ± 0.10
Planet density (g cm ⁻³)	1.26 ± 0.50	1.3 ± 0.3	1.3 ± 0.3	1.0 ± 0.4

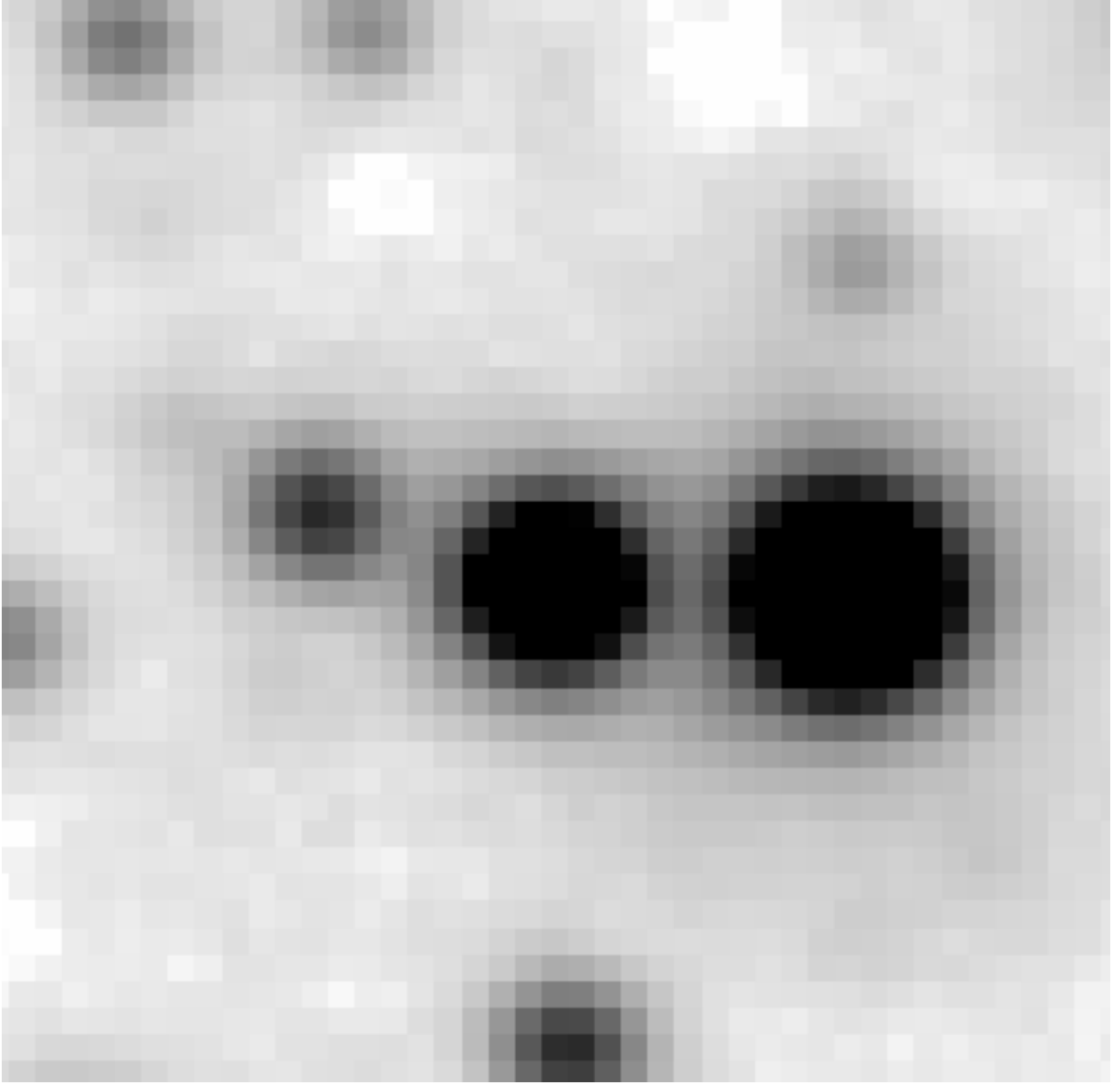


Fig. 1.— Portion of a SOFI K_s -band image including OGLE-TR-113 ($K_s = 13.00$), which is the bright star at the center. This image covers 12×12 arcsec, and the faintest stars seen have $K_s \sim 18$.

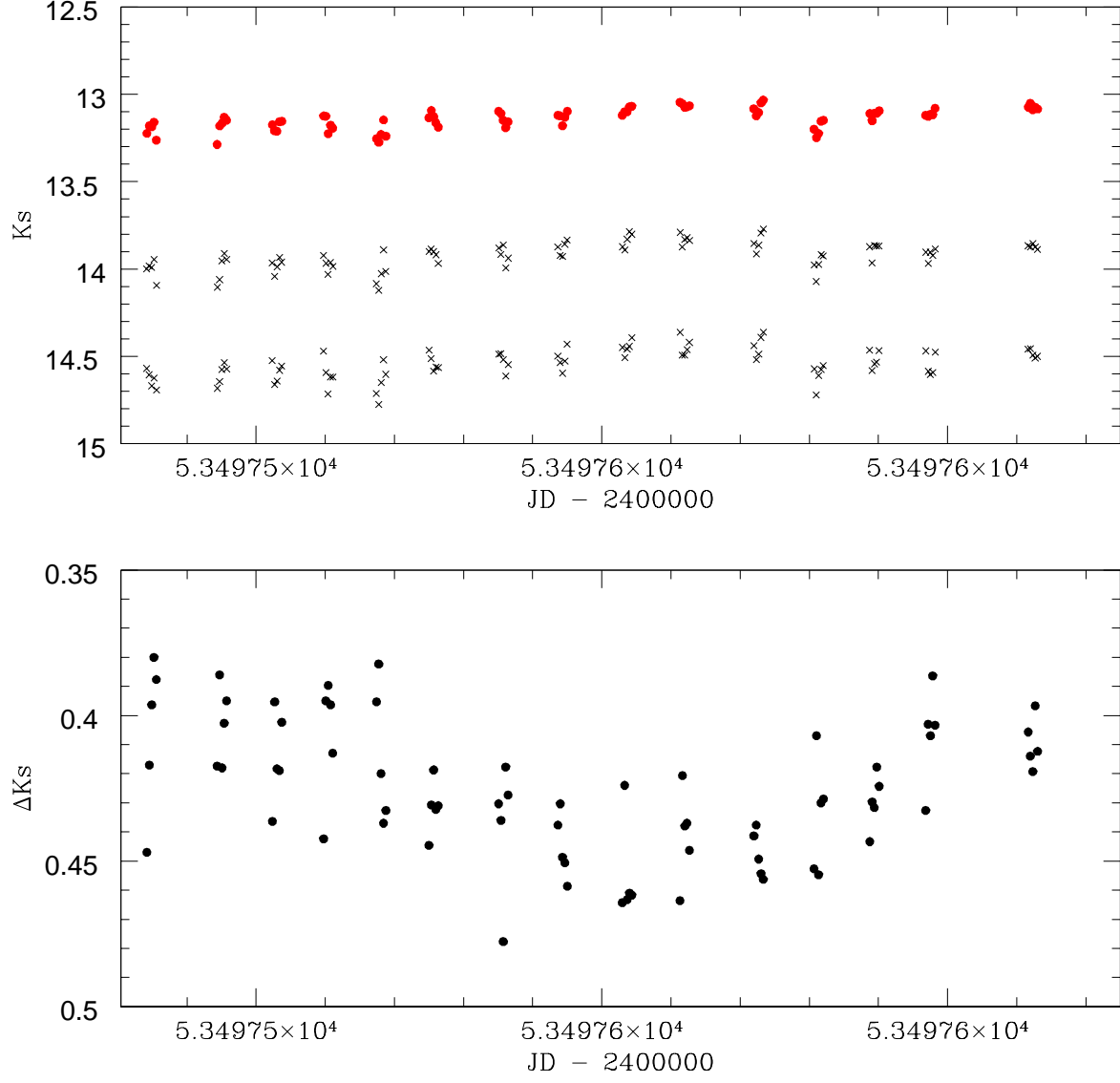


Fig. 2.— Top: Light curves of OGLE-TR-113 (circles) and two comparison stars (crosses) in the K_s -band. Bottom: Transit in the K_s -band.

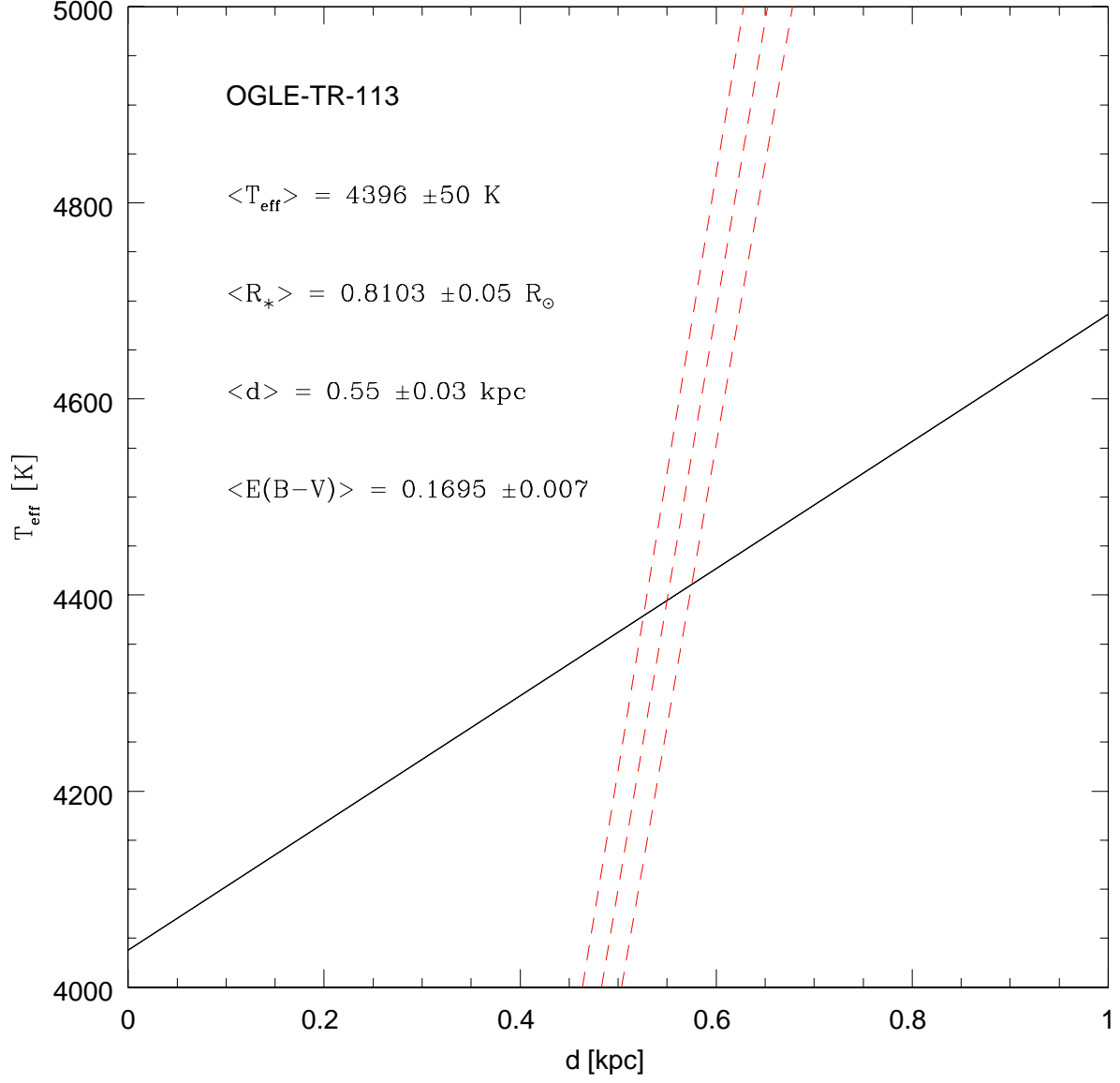


Fig. 3.— Effective temperature and distance for OGLE-TR-113b. The dashed (red) lines show the radius-temperature constrain for main-sequence stars (errors in the optical and infrared photometry are considered). Black lines give the temperature inferred from the surface brightness relations (see Gallardo et al. 2005, Section 4 for further explication).

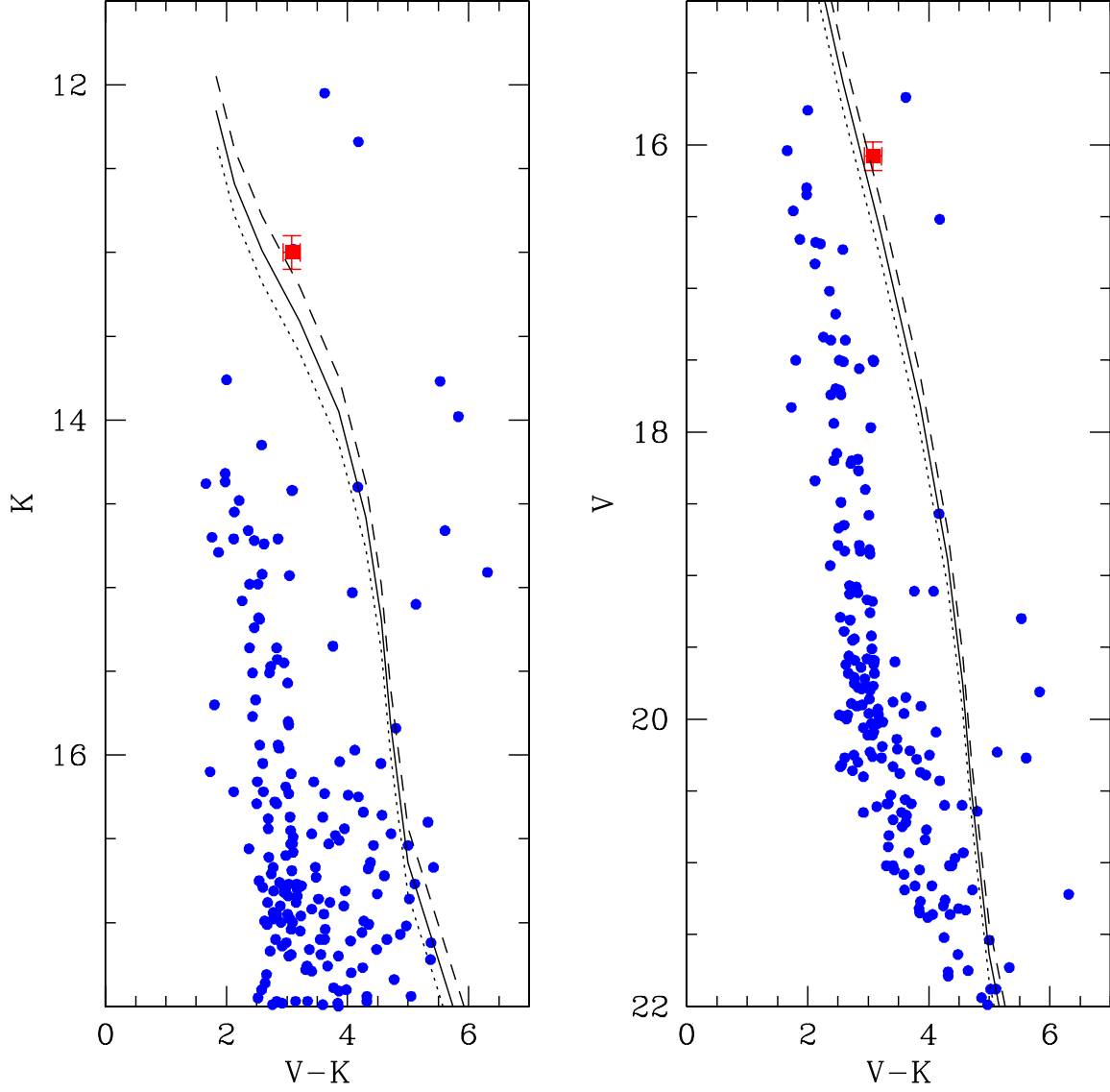


Fig. 4.— Optical-infrared color-magnitude diagrams of a $1' \times 1'$ field centered in OGLE-TR-113. The (red) filled square marks the location of OGLE-TR-113. Isochrones for solar age and metallicity, for different distances are also shown: $d = 550$ pc (solid line), $d = 600$ pc (dotted line) and $d = 500$ pc (dashed line).

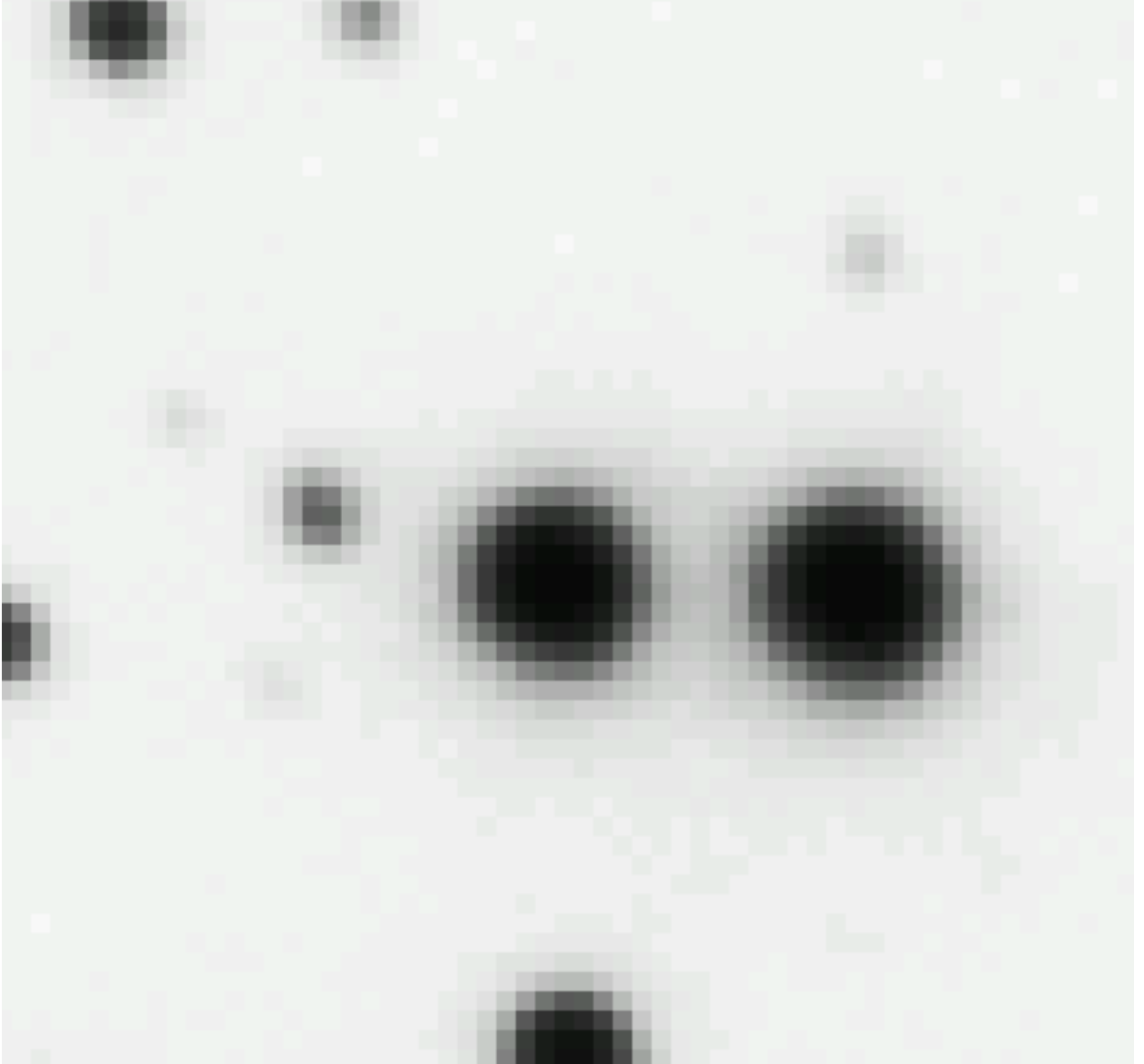


Fig. 5.— Portion of a 0.6 arcsec seeing VIMOS image including OGLE-TR-113 ($V = 16.08$), which is the bright star at the center. This image covers 12×12 arcsec as in Figure 1, and the faintest stars seen have $V \sim 24$.

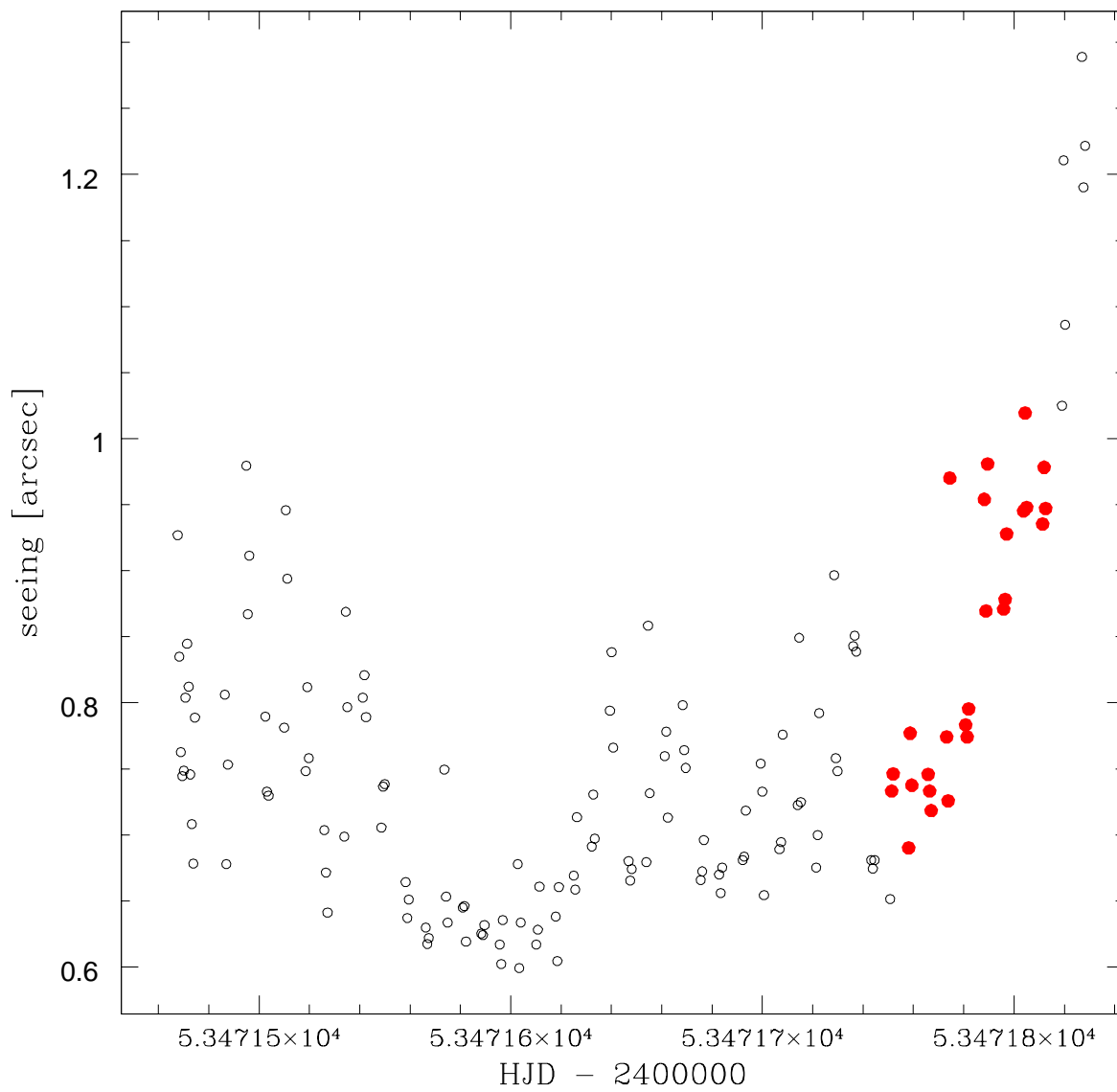


Fig. 6.— Seeing during the second observation night with VIMOS. The seeing remained below 1 arcsecond for most of the night. The filled (red) points correspond to the transit.

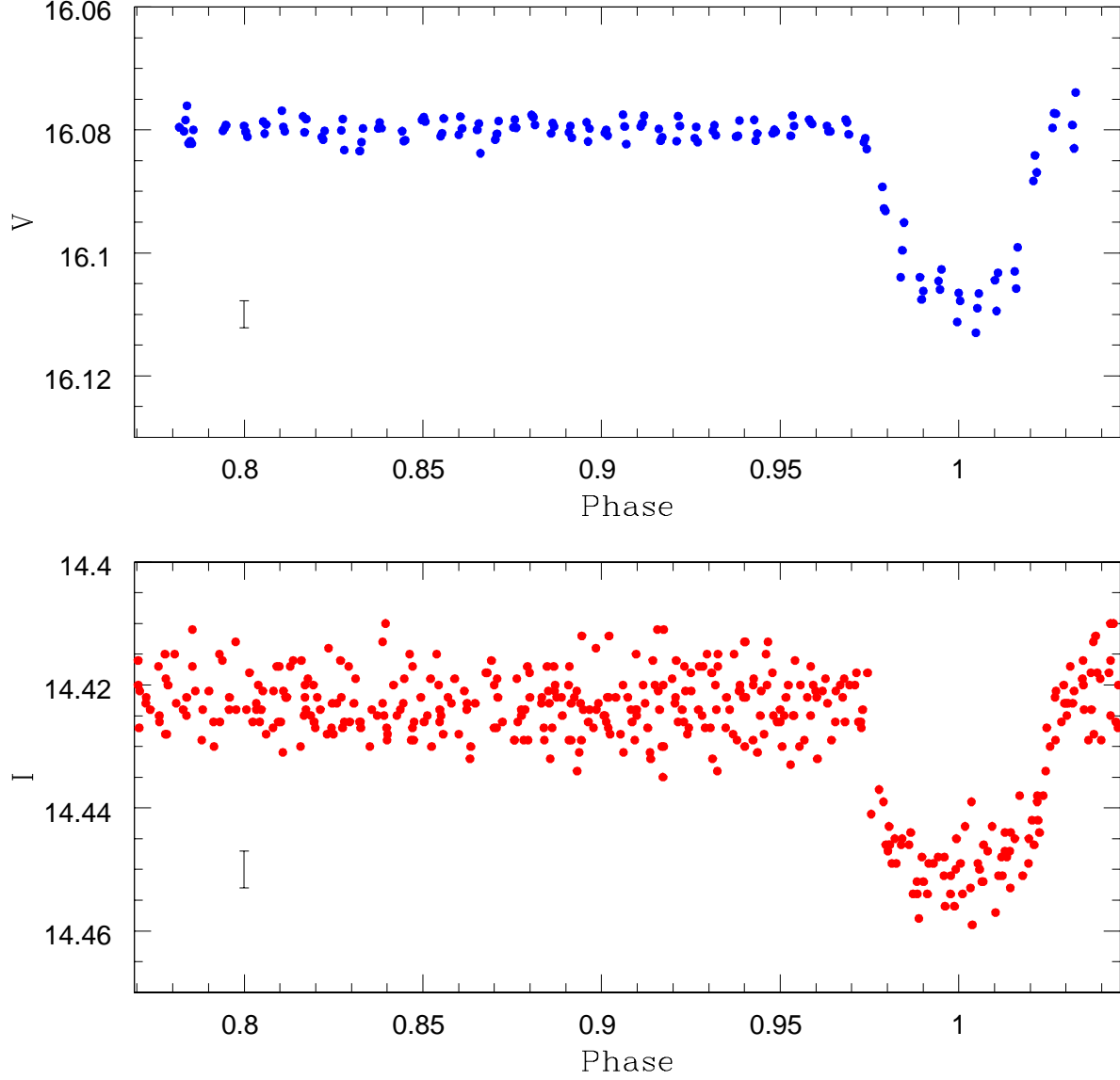


Fig. 7.— Single transit of OGLE-TR-113 observed during April 10th 2005 with VIMOS in the V-band (top) compared with the OGLE phased light curve transit in the I-band (bottom). Also shown is the size of the error bars. The smaller scatter of our photometry is evident.

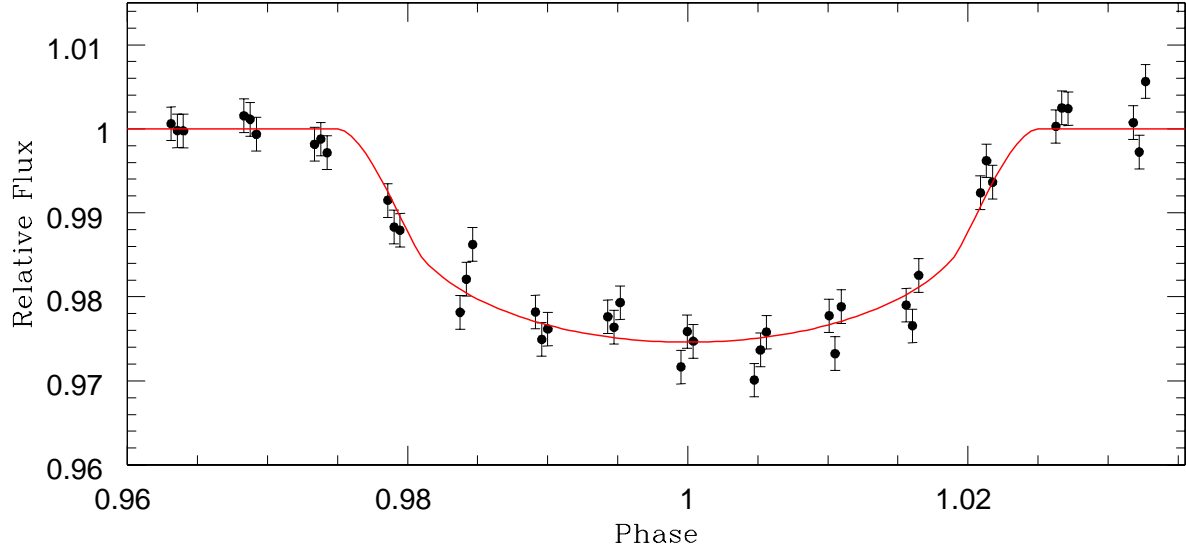


Fig. 8.— Fit to the single transit of OGLE-TR-113 in the V-band.

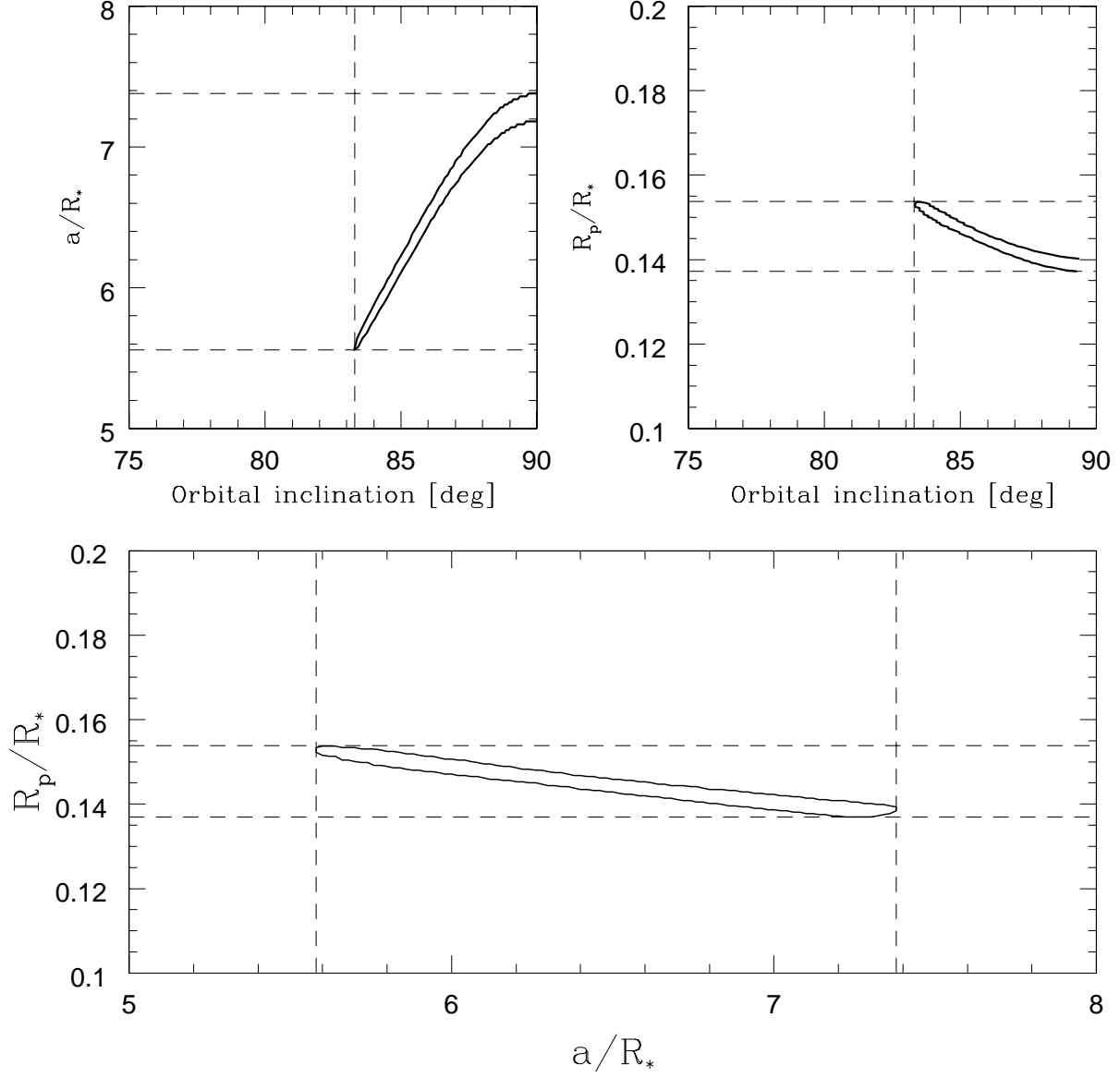


Fig. 9.— Regions with $\Delta\chi^2 \leq 1.25$ (see text) for the three possible projections of the fit parameters. The $\Delta\chi^2 \leq 1$ regions differ only slightly and are not plotted to avoid confusion.

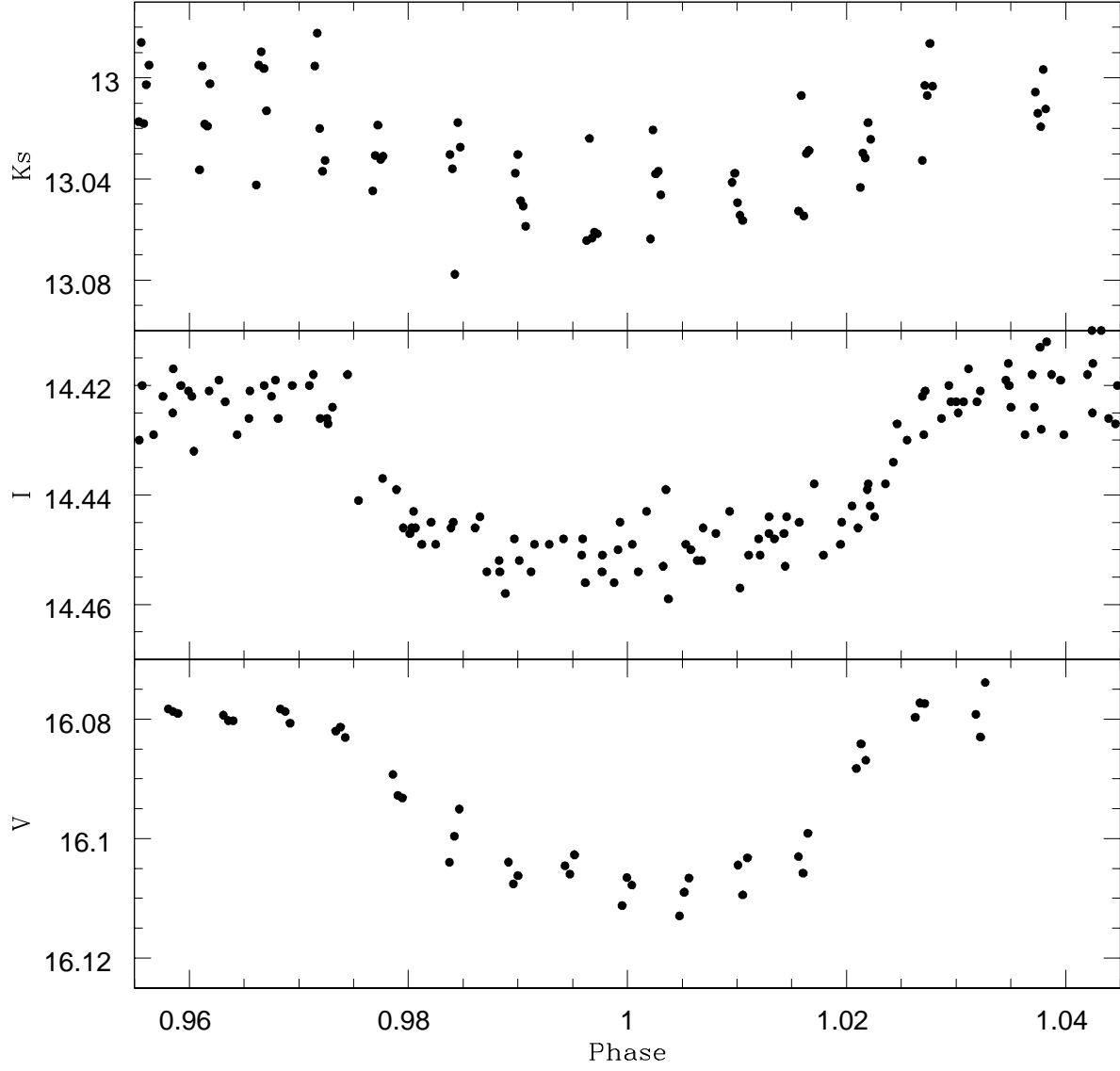


Fig. 10.— Comparison of an individual transit for OGLE-TR-113 in the K_s -band (top), the phased OGLE I-band light curve for several transits (middle), and another individual transit in the V-band (bottom). The duration and amplitudes of these transits are consistent with a planet.